X-Ray Absorption Spectroscopy combined with Time-Dependent Density Functional Theory elucidates differential substitution pathways of Au(I) and Au(III) with Zinc Fingers.

Camilla Abbehausen,[a,1] Raphael Enoque Ferraz de Paiva,[a] Ragnar Bjornsson,[b] Saulo Quintana Gomes,[a] Zhifeng Du,[c] Pedro Paulo Corbi,[a] Frederico Alves Lima,[d,1*] Nicholas Farrell[c,1]

[a] Institute of Chemistry, University of Campinas – UNICAMP, P.O. Box 6154, CEP 13083-970, Campinas, São Paulo, Brazil.

[b] Science Institute, University of Iceland, Dunhagi 3, IS-107 Reykjavik, Iceland

[c] Department of Chemistry, Virginia Commonwealth University, 1001 W. Main Street, Richmond, Virginia 23284-2006, United States.

[d] Centro Nacional de Pesquisa em Energia e Materiais, Brazilian Synchrotron Light Laboratory – LNLS, CP 6192, 13084-971 Campinas, SP, Brazil.

[1]Authors to whom correspondence should be addressed: npfarrell@vcu.edu; frederico.lima@xfel.eu and camilla.abb@gmail.com

[*]Current address: European XFEL GmbH, Holzkoppel 4, 22869 Schenefeld, Germany

Abstract

A combination of two element (Au, Zn) X-ray Absorption Spectroscopy (XAS) and time-dependent density functional theory (TD-DFT) allowed the elucidation of differential substitution pathways of Au(I) and Au(III) compounds reacting with biologically relevant zinc fingers (ZnFs). The C-terminal $Cys_2HisCys$ finger of the HIV-1 nucleocapsid protein NCp7, and the Cys_2His_2 human transcription factor Sp1, were probed by gold L_3-edge XAS. The computational studies accurately reproduced the experimental XAS spectra and allowed the proposition of structural models for the interaction products at early time points. The use of known model compounds helped assign oxidation states and the identity of the gold-bound ligands. In the case of $[AuCl(PEt_3)]$, interaction with the NCp7 confirmed a linear P-Au-Cys coordination sphere after zinc ejection whereas for the Sp1, loss of PEt_3 results in linear Cys-Au-Cys or Cys-Au-His arrangements. These reactions may be considered as result of direct electrophilic attack on the zinc finger by the highly thiophilic Au(I). Reactions with Au(III) compounds on the other hand showed a variety of possible binding modes where the final Au(I) products vary depending on zinc finger and allowed identification of distinct ligand binding and Au(III) reduction. Prompt reaction between $[AuCl(dien)]^{2+}$ and $[Au(dien)DMAP]^{3+}$ with Sp1 showed a partially reduced Au center and a final linear His-Au-His coordination. On the other hand, in presence of NCp7, $[AuCl(dien)]^{2+}$ readily reduces to Au(I) and changes from square-planar to linear geometry with Cys-Au-His coordination, while $[Au(dien)DMAP]^{3+}$ initially maintains its Au(III) oxidation state and square-planar geometry and the same first coordination sphere. The latter is the first observation of a "non-covalent" interaction of an Au(III) complex with a zinc finger and confirms early hypotheses that stabilization of Au(III) occurs with N-donor ligands. Modification of the zinc coordination sphere, suggesting full or partial zinc ejection, is observed in all cases irrespective of whether Au(I) or Au(III) is used, and for $[Au(dien)(DMAP)]^{3+}$ represents a novel mechanism for nucleocapsid inactivation. The combination of XAS and TD-DFT calculations in this study presents the first direct experimental observation that not only compound reactivity, but also ZnF core specificity can be modulated based on the coordination sphere of Au(III) compounds.

Keywords: Zinc finger proteins, gold complexes, X-ray absorption spectroscopy, TD-DFT.

Introduction

Zinc finger (ZnF) proteins are increasingly recognised for their relevance and importance in diseases. Zinc finger proteins are the largest transcription factor family in the human genome and there is increasing evidence for their role in cancer progression.[1] Several zinc fingers are also involved in immune regulation through effects on cytokine production and other inflammatory mediators.[2, 3] In antiviral therapy, a desirable target is the HIV nucleocapsid protein 7 (NCp7), which would complement current anti-retroviral therapies.[4, 5] In considering specific ZnFs as targets for therapeutic intervention the structural diversity of the zinc coordination motifs represents a considerable challenge to specificity.[6] In this paper we show how X-ray Absorption Spectroscopy (XAS) combined with Density Functional Theory studies (DFT) can be used to examine the effects of the zinc cooordination sphere (Cys_2His_2 *versus* $Cys_2HisCys$) in dictating reactivity and in delineating the intimate mechanisms of substitution on a ZnF template with multiple ligand binding sites available.

Zinc fingers are excellent templates for metal ion replacement[7] and their interaction with metal complexes is an important component of bioinorganic and medicinal inorganic chemistry. Platinum, cobalt and gold compounds have all been designed to attack specific zinc fingers (domains or cores) by a variety of mechanisms.[7-9] Recently, gold compounds have received intensive attention due to their promising cytotoxic and potential anticancer properties. They have been rationalized as an alternative to cisplatin. A number of possible molecular targets have been suggested for gold allowing for rational design using molecular biology allied to modern spectroscopic techniques to enhance specificity.[10-12] Early studies on the anti-arthritic action of Au(I) and Au(III) compounds suggested interactions with zinc fingers followed by zinc ejection and formation of the so-called *gold fingers*.[13-15] Reactions of gold compounds with zinc fingers are generally very fast and even ESI-MS spectra at earliest time points show mixtures of species.[13-15] Gold compounds act as Lewis acid electrophiles by covalent binding to cysteines or histidines of the ZnF core. The reactivity of Au(I) in the general structure $[AuX(PR_3)]$ can be tuned by variation of leaving group X and/or altering the steric and electronic properties of the phosphine.[14, 16, 17] In the case of Au(III), the oxidation state of incorporated gold from a variety of complexes is +1, thus implicating concomitant oxidation of the peptide core. The properties of $[AuX(dien)]^{n+}$ (*dien,* $(NH_2CH_2CH_2NHCH_2CH_2NH_2$, tridentate diethylenetriamine) can also be

modulated by varying the nature of the ligand in the fourth coordination site using $AuClN_3$ or AuN_4 compounds.[18-20] Apart from these series, a variety of Au(III) compounds has been studied as ZnF inhibitors, but the structural details of the products formed still require full elucidation, especially the question of when reduction to Au(I) occurs, hindering a mechanistic description of the Zn ejection process.[21-24]

In this study the interaction of Au(I) and Au(III) complexes with zinc finger peptides was investigated using the Au L_3- and Zn K-edge XAS in combination with time-dependent density functional theory (TD-DFT) calculations. In the case of XAS, the samples were frozen in liquid nitrogen as soon as the mixture was placed in the sample holder (less than one minute of manipulation) and kept at 50 K during the course of the measurements. The immediate freezing of the reaction samples for XAS allows for a snapshot of the very early reaction profiles, complementing other spectroscopic studies. With suitable control samples, Au(I) and Au(III) can be easily distinguished and, when combined with two-element studies probing the Zn coordination sphere, the initial steps of the interaction can be distinguished. Model peptides of the C-terminal zinc finger domain of HIV NCp7, (from here on in referred as NCp7), and the N-terminal finger F3 of the human transcription factor Sp1, (from here on called Sp1), were compared. They represent two different ZnF families, NCp7 being the -Cys-X_2-Cys-X_4-His-X_4-Cys- ($Cys_2HisCys$) motif while the Cys-X_2-Cys-X_{12}-His-X_3-His- (Cys_2His_2) is the coordination sphere of Sp1, Fig. 1. The peptides differ in their electronic and steric properties with respect to cysteine nucleophilicity and availability.[25, 26] The intimate behaviour of Au(I) and Au(III) compounds acting as Lewis acid electrophiles is shown to be dependent on the compound and on the specific ZnF core. The use of $[Au(dien)DMAP]^{3+}$, (DMAP = 4-dimethylaminopyridine ($NC_5H_4N(CH_3)_2$), with a relatively substitution-inert AuN_4 coordination sphere, allowed the first observation of a "non-covalent" Au(III)-ligand moiety in the presence of NCp7 but not Sp1. Dual-element XAS using Zn K-edge XAS data confirms the simultaneous modification of the Zn coordiantion sphere. The stabilization of an Au(III)-ligand moiety in the presence of a ZnF illustrates the ability to modulate the Au(III)-ZnF reaction by suitable ligand choice and of ZnF itself. The compound $[Au(dien)DMAP]^{3+}$ and its congener $[Au(dien)(9\text{-}EtGua)]^{3+}$ inhibit RNA binding to the "full" HIV nucleocapsid protein (NC) and are moderate inhibitors of HIV infectivity.[27] Therefore, the XAS studies suggest that the compounds may be situated as a novel class of "non-covalent" zinc ejectors, followed eventually by gold-peptide bond formation.[4, 28]

The combination of XAS and TD-DFT used here is a robust approach that can be extended to studies about the interaction of virtually any metallodrug with a metalloprotein target, particularly in the case of spectroscopically inert Zn(II).

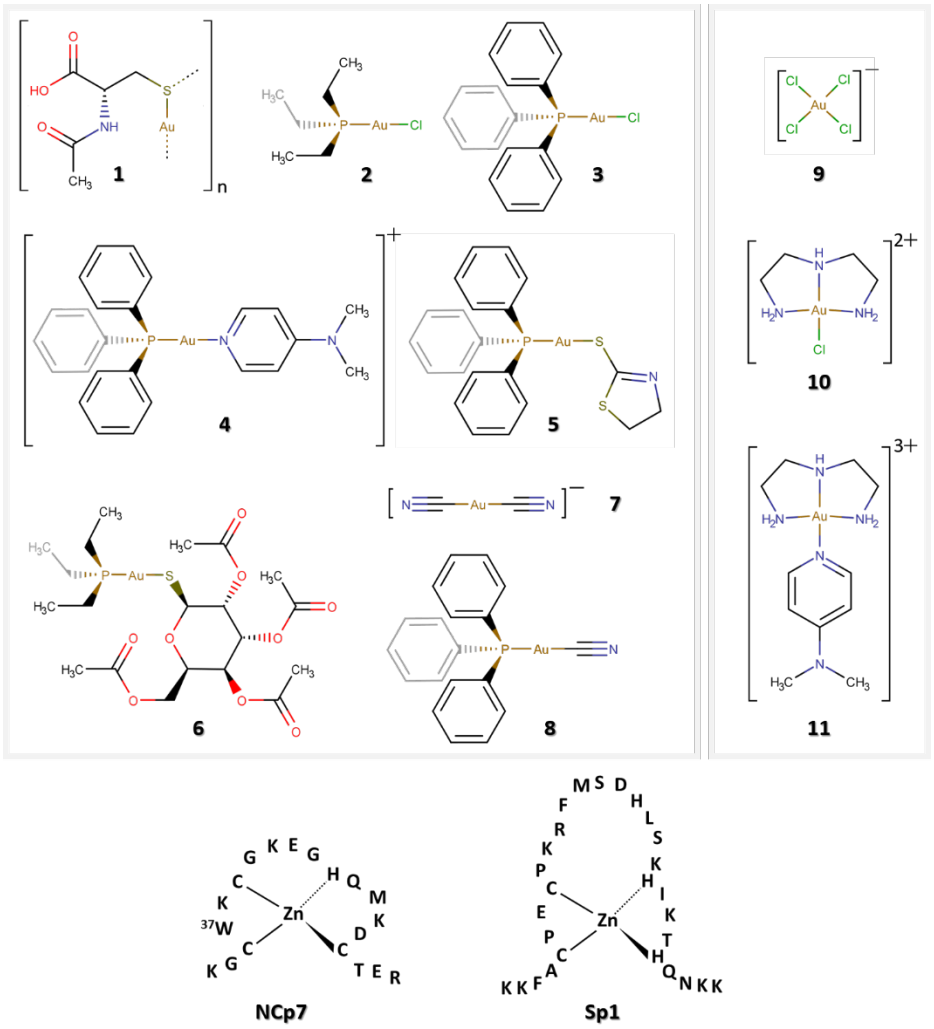

Figure 1. Structural formulas of the model Au compounds used in this study. Compounds **1**-**8** are Au(I) and compounds **9**-**11** are Au(III). Compound **1** is known to possess a polymeric structure. The zinc finger model peptides NCp7and Sp1 are also shown.

Experimental

Synthesis and zinc finger preparation

Complexes **1, 3**-**5**, **8**, **10** and **11** were synthesized and purified according to literature procedures.[16, 20, 28-30] The crystal structures of all compounds, except **1**, **4** and **11**, have been

already reported elsewhere.[28, 29, 31-37] Compounds **2**, **6**, **7** and **9** were acquired from Sigma-Aldrich and used without further purification. Characterization of the synthesized compounds (**1, 3-5**, **8**, **10** and **11**) were performed by conventional spectroscopic techniques including ^{1}H, ^{13}C, ^{31}P NMR spectroscopy, mass spectrometry, elemental analysis, and infrared and UV spectroscopies, attesting the success of the syntheses and their integrities.[16, 30]

The zinc finger models used in this study were the second finger HIV-1-NCp7 and third finger Sp-1. The apopeptides were purchased from Aminotech Co. (São Paulo, Brazil) and they have the following sequences: NCp7 (F2) (KGCWKCGKEGHQMKNCTER), monoisotopic mass 2224.47 Da; Sp1 (F3) (KKFACPECPKRFMSDHLSKHIKTHQNKK), monoisotopic mass 3366.95 Da. The apopeptides were checked by mass spectrometry and used as received. Both zinc fingers were prepared by dissolving sufficient mass of apopeptides in a 100 mmol L^{-1} solution of zinc acetate prepared in degassed water. The total volume was achieved by adding acetate buffer pH 7.4 to a final concentration of 30 mmol L^{-1} of zinc finger.

Sample preparation

The solid samples of compounds **1**-**9** used in the XAS measurements were finely grounded and diluted in boron nitride to a maximum X-ray absorbance of about 1. Then, they were pressed into circular pellets of 13 mm diameter using a hydraulic press, placed in a plastic sample holder and covered with polyimide adhesive tape (Kapton) with about 40 μm thickness. Gold L_3-edge XAS measurements of the complexes **1**-**9** were performed in solid state at XAFS1 beamline.

Stock solutions of [AuCl(PEt_3)] (**2**) and auranofin (**6**) were prepared by dissolving the solid compounds in dimethylformamide (DMF) to a final concentration of 100 mmol L^{-1}. For evaluating the interaction of the model compounds with the zinc fingers, a total sample volume of 10 μL of the Au(I) models **2** and **6** were prepared by mixing sufficient volumes of the solutions of model compounds to each zinc finger solution (NCp7(F2) and Sp1(F3)) in a molar ratio of 1:1. A similar procedure was employed in the preparation of the Au(III) interaction products (**10** and **11**) with both NCp7 (F2) and Sp1 (F3) zinc fingers. The *gold finger* sample (AuF) from Sp1 (F3) was obtained incubating [AuCl(PEt_3)] with Sp1-ZnF3 in a 1:1 molar ratio for 1h. The reaction mixture was purified using a Waters 515 HPLC instrument with a reverse

phase Phenomenex Jupiter C_{18} column (5μm, 250 mm×4.6 mm, 300 Å) and a 100 μL sample injection loop. Flow rate of 1 mL/min was used for all the experiments. Gradient is as follow: 0-30min, 10-80% B. A is H_2O with 0.1% TFA, and B is acetonitrile with 0.1% TFA. UV detection wavelengths were 280 nm and 220 nm. The composition of the isolated fraction was further characterized by ESI-MS. The eluent from the collected sample was lyophilized and the solid was redissolved in ammonium phosphate buffer prior to XAS measurements. A sample with final concentration of 48 μM was used.

In each XAS measurement of the samples in solution, about 3 μL of the prepared solutions of the zinc fingers and the Au(I,III) interaction products (**2**, **6**, **10** and **11**) were placed in a plastic sample holder, covered with the same 40 μm thick Kapton adhesive and frozen in a closed-cycle liquid helium cryostat. The solution samples were kept below 50 K during these measurements. Inspection of fast XANES scans revealed no signs of radiation damage, and the first and last scans of each data set used in the averages were identical. The complexes **10** and **11** (100 μM), the isolated zinc fingers and the respective interaction products with the Au(I,III) models were measured in aqueous solution at the XAFS2 beamline.[38]

Data averaging, background subtraction and normalization were done using standard procedures using the ATHENA package.[39]

XAFS1 and XAFS2 beamlines

Both beamlines are located at the Brazilian Synchrotron Light Laboratory (CNPEM/LNLS).[38, 40] At the XAFS1 beamline the incident energy was selected by a channel-cut monochromator equipped with a Si(111) crystal, and at the the XAFS2 beamline a double-crystal, fixed-exit monochromator was used. The beam size at the sample was approximately 2.5 x 0.5 mm^2 (hor. x vert.) at XAFS1 and 0.4 x 0.4 mm^2 at XAFS2, with an estimated X-ray flux of 10^8 ph/sec (XAFS1) and 10^9 ph/sec (XAFS2). The incoming X-ray energy was calibrated by setting the maximum of the first derivative of L_3-edge of a gold metal foil to 11919 eV. The XAS spectra of the solid samples (complexes **1**-**9**) were collected in conventional transmission mode using ion chambers filled with a mixture of He and N_2. In the case of the samples in solution, fluorescence mode detection was used. The fluorescence signal was recorded using a 15-element Ge solid-state detector (model GL0055S – Canberra Inc.) by setting an integrating window of

about 170 eV around the Au $L\alpha_1$ and $L\alpha_2$ emission lines (9713.3 eV and 9628.0 eV, respectively). Zinc K-edge XAS were also collected for the isolated zinc fingers and the respective reaction products of Au(III) models **10** and **11** with both NCp7(F2) and Sp1(F3) zinc fingers. Zn K-edge XAS data of only interaction of Au(I) compound **2** with NCp7(F2) could be measured. These data were also recorded in fluorescence mode at XAFS2 beamline using the same 15-element Ge solid-state detector and setting an integrating window of about 170 eV around the Zn $K\alpha_1$ and $K\alpha_2$ emission lines (8637.2 eV and 8614.1 eV, respectively). In the Zn K-edge XAS experiments the incoming energy was calibrated by setting the absorption edge of a Zn foil to 9659 eV.

EXAFS fitting for auranofin

The EXAFS fit of auranofin (**6**) was performed in k-space in the interval 2.84-10.65 $Å^{-1}$, using the Artemis package.[39] This was enough to accurately determine the first coordination shell around the gold center (linear: P-Au-S). FEFF version 6 was used to calculate the scattering paths based on the auranofin crystalline structure.[37] The structural parameter obtained in the EXAFS fit are given in Table S2.

TD-DFT

Calculations were performed on all Au(I,III) compounds (**1**-**11**) to see if our protocol could reproduce the trends in energy shifts and intensities. A comparison of experimental L_3-edges vs. TDDFT-computed L-edges is shown in Figures S2 and S3 and show overall good agreement with the experimental data. All calculations were performed using the ORCA quantum chemistry code, version 3.0.3.[41]

All molecules were optimized at the PBE0/def2-TZVP level of theory using the def2-ECP effective core potential.[42] TDDFT calculations (using the Tamm-Dancoff approximation) as implemented in ORCA[43] were performed with the PBE0[43-45] functional using an all-electron scalar relativistic Douglas-Kroll-Hess Hamiltonian[46-48] with the DKH-def2-TZVP-SARC basis set.[49] The Au 2p to valence excitations were performed by only allowing excitations from the Au 2p donor orbitals to all possible virtual orbitals of the molecule (only limited by the number of calculated roots). Intensities include electric dipole, magnetic dipole and quadrupole

contributions. The RIJCOSX approximation [50, 51] was used to speed up the Coulomb and Exchange integrals in both geometry optimizations and TDDFT calculations.

Mass Spectrometry

1mM interaction products were obtained by mixing at room temperature an Au(I) complex stock solution with the corresponding ZnF stock solution (1 eq of Au complex per ZnF core, water/acetonitrile mixture, pH 7.0 adjusted with NH_4OH if needed). MS experiments were carried out on an Orbitrap Velos from Thermo Electron Corporation operating in the positive mode. Samples (25 μL) were diluted with methanol (225 μL) and directly infused at a flow rate of 0.7 μL/min using a source voltage of 2.30 kV. The source temperature was maintained at 230°C throughout.

Blue Star Sting[52]

The amino acid relative accessibility is calculated according to SurfV program[53]. Numerical values are expressed in $Å^2$. Electrostatic potential values are calculated using Delphi[54] program according to the modifications made by Walter Rocchia[55] and further adapted to Java Protein Dossier requirements[56]. The numerical values are expressed in kT/e.

Results and Discussion

Eight Au(I) complexes, representing X-Au-Y coordination spheres (with X, Y = S, P, Cl and N) and three model Au(III) complexes, Fig. 1, had their Au L_3 near-edge XAS spectra (also referred to as X-ray Absorption Near-Edge Spectroscopy region – XANES) evaluated. The choice of these models was based on their linear P-Au-S, S-Au-S, P-Au-N and even P-Au-C coordination spheres around the gold metal, to aid in understanding the XAS spectra of the Au/ZnF adducts of interest. The Au(PEt_3) compounds **2** ([AuCl(PEt_3)], (Et = CH_3CH_2) and **6** (auranofin, where the "leaving group" is 2,3,4,6-tetra-O-acetyl-1-thio-β-D-glucopyranosato-S ligand) were chosen because of their structural similarities but different kinetic reactivity.[28, 37] Au(III) compounds, $[AuCl_4]^-$ (**9**), $[AuCl(dien)]^{2+}$ (**10**) and $[Au(dien)(DMAP)]^{+3}$ (**11**) were selected because the use of N-donors, such as chelating ligands, nucleobases or simple planar

amines in gold compounds, has been suggested to stabilize the Au(III) oxidation state, even in the presence of peptides with high cysteine content such as ZnF.[19, 20] Details of all experimental methods are given in the Supplemental Information.

In general, the XAS spectra of the model compounds present the expected white line peak at about 11921 eV and 11923-11925 eV (in the case of Au(III) and Au(I), respectively). In the case of Au(III) ($5d^8 6s^0$ electronic configuration) the peak originates from the dipole-allowed $2p_{3/2} \rightarrow 5d$ transitions characteristic of L_3-edges, but similar whitelines have also been seen for Au(I) [$5d^{10}6s^0$] valence configuration, suggesting perhaps some unoccupied d-orbital character to be present as suggested by previous studies[57, 58] or perhaps being due to other transitions (see TD-DFT discussion below). In a first approximation, using an atomic orbitals picture, rather than invoking molecular orbitals, is sufficient to explain the proportionality of the intensity of the L_3-edge XAS white line and the metal d-electron hole count. This simple picture allows the inference of the metal oxidation state in many cases. However, occasionally other effects cannot be properly accounted for, e.g., charge-transfer transitions, shake up/down, etc. [59, 60] A detailed analysis of the XAS spectra of the model compounds including a summary of the spectroscopic features observed for each compound is given in Supplementary Information (Figure S1, Table S1). Figures S2 and S3 compare the experimental and the TD-DFT calculated Au L_3-edge spectra obtained for all model Au(I) and Au(III) compounds. Briefly, the trends in Au(I) compounds are consistent with the understanding of ligand effects. Despite their similarity, by comparing the XANES of compounds **2**-**5** it is possible to explain the lower white line intensity of [$AuCl(PPh_3)$], followed by [$AuCl(PEt_3)$] (compounds **3** and **2,** respectively), as a consequence of chloride's p-donor character. Furthermore, the Ph_3P ligand is a weaker σ donor than Et_3P. The intense white lines of compounds **7** and **8**, unusual for the Au(I) case, reveal a substantial amount of unoccupied d-orbital character in those complexes, rationalized by the interaction of Au(I) d orbitals with π* orbitals from CN^-. The electronic structure of Au-CN^- compounds is of interest due to the formation of {$(NC)_yAu_x$-NCp7} ($x,y \leq 3$) in the reaction of Au(I)-mercaptothiazoline compounds with the C-terminal NCp7.[61] The electronic structure is also of interest in the broader context of the effect of CN^- on biodistribution of gold and the observation of $[Au(CN)_2]^-$ as a common metabolite of Au(I) drugs.[62, 63] Au(III) compounds show the highest white line peaks in the series investigated, as a consequence of empty d orbitals promoting the allowed $2p_{3/2} \rightarrow 5d$ transitions in the L_3-edge XAS, again having a simplistic atomic orbital picture in mind. As

stated previously, the intensity of the white line can be used as a fingerprint of the d-electron count in these cases; however, in some cases (e.g., very covalent systems or when significant charge-transfer is present) the standard relationships between experimental Au L_3-edge white line intensities and oxidation state do not hold.[60] The XANES spectrum of compound **9** ($[AuCl_4]^-$) contains a sharp peak in the white line region and presents a distinct XANES spectrum when compared to the compounds **10** and **11**, $[AuCl(dien)]^{2+}$ and $[Au(dien)(dmap)]^{3+}$, respectively. Compounds **10** and **11** have their white line maxima shifted by 0.8 and 1.0 eV to lower energy respectively, in comparison to compound **9**, indicating that the *dien* ligand has an oxidative effect (larger number of gold d holes) on the Au center. This confirms a higher stability of Au(III) species bound to chelating N- donor ligands and the effect of $AuClN_3$ *versus* AuN_4 coordination spheres, which could be important in biological reducing media.[19, 20] Point symmetry also plays a role in giving intensity to the white line in the gold L_3 XAS.

Interaction of Au(I) compounds with ZnFs

The dominant species in the ESI-MS spectrum of **2** with NCp7 (hereafter called **2+NCp7**) after short incubation times (measured as soon as possible after reaction) are attributed to the removal of zinc and coordination of the {(Et_3P)Au} species to the peptide, called here (Et_3P)Au-apopeptide. Signatures of Au-apopeptide, *gold finger* (AuF), representing the loss of Et3P group and the original zinc finger (ZnF) are also observed.[16,17] The ^{31}P NMR spectrum of the interaction at early time points shows two new ^{31}P peaks, whose chemical shifts can be attributed to displacement of the Cl^- ligand by a sulfur donor ligand, as previously observed for $[AuCl(PPh_3)]$.[16] In the case of Sp1 (hereafter called **2+Sp1**), a remarkably clean MS spectrum is obtained containing signatures of only *gold finger*.[17] This motivated the purification of the {AuF} produced in the interaction of **2+Sp1** and its concurrent investigation by MS and XAS. Details about the purification protocol are given in the Supplementary Information.

NCp7. Figure 2 shows the Au L_3-edge XANES spectra of the Au(I) model compounds **1, 2** and **6** and the interactions of **2** with the NCp7 and Sp1 zinc fingers. Compound **2** presents an Au XANES spectrum similar to the other Au(I) compounds with P-Au-Y coordination (where Y can be Cl, N or S), with a white line peak located at 11924.2 eV and about 0.83 normalized units. After interaction with NCp7, the XANES of the resulting product **2+NCp7** changes slightly: the

broad and weak white line sharpens and gains intensity, peaking at 11925.7 eV and 0.97 normalized units. This final spectrum is almost identical to that of auranofin itself (**6**), which has a peak at the same energy and only slightly more intense (0.98 units), indicating similar geometry and electronic configuration between these species.

The spectrum of auranofin in the presence of NCp7 product showed no discernible difference to auranofin itself, presenting the same P-Au-S coordination sphere and suggests that no displacement occurred at this early time point.[12] However, over time, ^{31}P NMR spectroscopy did show slow reaction.[17] Displacement could be followed over time in subsequent experiments. The result is also consistent with our interpretation that the reaction is kinetically much slower than that of **2**.[12] As the near-edge XAS region is sensitive to both the atomic arrangement and the electronic structure around the metal,[64-67] the data confirm that the product from **2** + NCp7 presents a P-Au(I)-S coordination. The proposed PEt_3-Au-Cys coordination is further supported by the inspection of the EXAFS (Extended X-ray Absorption Fine Structure) of **2+NCp7** which is virtually superimposable with that of free auranofin (compound **6**) up to k=10 $Å^{-1}$ (Table S2 and Figures S4 and S5). Travelling Wave Ion Mobility spectra of the {AuF} species formed from **2+NCp7** indicated the presence of Cys-Au-Cys conformers, which is a consequence of the multiple possible cysteine binding sites.[17] The formation of such conformers can now be readily understood by first the immediate formation of different {(PEt_3)Au-F} species as confirmed here followed by loss of the PEt_3 ligand and formation of a second Au-Cys bond.

Sp1. The XANES of **2+Sp1**(AuF) differs considerably from that of compound **2** and **2+NCp7**, Figure 2 and 3(a). The white line region of **2** contains a broad and weak peak, which splits in two in the interaction product **2+Sp1**(AuF), with an energy separation of about 5.5 eV (see Table S1). The weak double feature in the white line of **2+Sp1**(AuF) (around 11924-11929 eV) is also evident in the XANES of compound **1** ([Au(nac)], with nac = N-acetyl-L-cysteine), which contains an S-Au-S environment. In the post-edge region of **2+Sp1**(AuF) a single broad feature is present, contrasting with the two marked structures observed in the spectra of **6**, **6+NCp7** and **2+NCp7**. Since a similar single feature is also observed in the spectrum of **1**, we can infer at first glance that the purified gold-finger could have a similar structure as compound **1**, *i.e.*, a S-Au(I)-S coordination. The EXAFS of **2+Sp1**(AuF) essentially overlaps with that of compound **1** up to k=8 $Å^{-1}$ (Figure S6). The apparently slightly shorter bond distance in the first

coordination shell of AuF suggested by EXAFS and the differences in the white line of **2+Sp1**(AuF) and compound **1,** could be explained by the formation of a shorter and more covalent Au-S bond in the pure gold finger or perhaps a slightly different local geometry in **2+Sp1**(AuF) than in compound **1**. Geometry optimizations using DFT of a single molecule of compound **1** (nac-Au-nac) gave an approximately linear S-Au-S geometry (S-Au-S angle of 177°). The peptide in AuF, however, may impose a different S-Au-S angle that may deviate more from linearity.

This suggestion contrasts with the conclusions from Travelling Wave Ion Mobility mass spectral study, which suggests a Cys-Au-His coordination environment for {AuF} formed from **2+Sp1**.[17] In the latter case, the gas-phase product ion was isolated and immediately subjected to further analysis, whereas in the present case we are dealing with an isolated product. Therefore, discrepancies may reflect kinetic *versus* thermodynamic preferences given the two methodologies, which have not been seen in these systems so far. The Cys-Au-His electronic structure is in fact very similar to that of Cys-Au-Cys (see **I-B** and **I-D** of Figure 4(b) below) and may also explain the spectra and the differences from model compound **1**. What is clear is the lack of any contribution from the {Au(PEt_3)} moiety, in line with previous results.[16, 17]

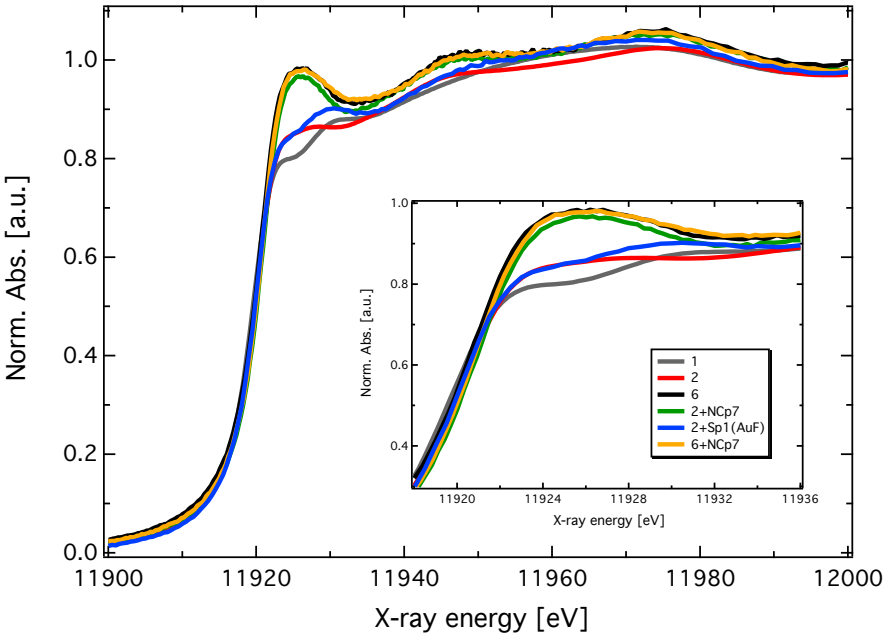

Figure 2. XANES spectra of the selected Au(I) model compounds and the products of the interaction with NCp7 and Sp1. Compound **1** (S-Au-S coordination) is also shown for comparison. The inset shows a zoom-in of the white line region, highlighting the spectral changes after interaction with the ZnFs.

TD-DFT. To provide a quantitative description of the interaction products of the Au(I) and Au(III) compounds with the ZnFs, we have employed DFT structural modeling and TD-DFT calculations of the Au L_3-edge XAS. TD-DFT calculations of metal K-edge XAS spectra have become popular and have been found to reproduce important pre-edge spectral features of metal complexes and cofactors well.[68-74] While L-edge spectra of first-row transition metals require more sophisticated wavefunction theory calculations that account for the difficult multiplet effects and spin-orbit coupling involving p- and d-shells, it has been found that a TD-DFT approach, neglecting both spin-orbit coupling and multiplet effects, works well for L-edges of second-row transition metals such as molybdenum and ruthenium where the multiplet effects should be small due to the larger spin-orbit coupling.[64,72] For Au, a third-row transition metal with an even larger spin-orbit coupling constant, this approach would be expected to work even better as the large spin-orbit coupling should result in even smaller mixing of spin-orbit split states. The Au(I) model compounds evaluated in this work had their structures optimized using DFT. More specifically, compound **1** was modelled as an almost linear nac-Au-nac model, while **2**, **5** and **6** had their structures optimized starting from the available crystal structures.[28, 37] Optimized structures are shown in Figure S2. Theoretical models of the interaction products were also created based on Et_3P-Au(I)-Cys (**I-A**), Cys-Au(I)-Cys (**I-B**), His-Au(I)-His (**I-C**) and Cys-Au(I)-His (**I-D**) coordination motifs with Cys being modelled as N-acetyl-N-methylamide-cysteine and His residues modelled as 5-methylimidazole (Figure 3). TDDFT calculations used a similar protocol as previously used for Mo L-edge spectra.[75] Additional details about the geometry optimizations and TD-DFT calculations are given in the Supplementary Information.

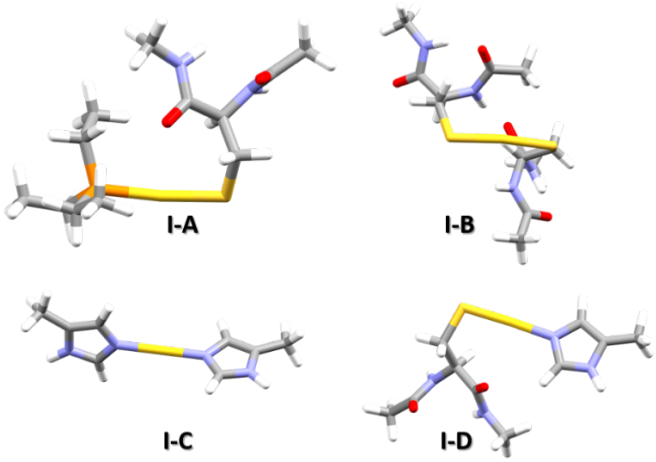

Figure 3. DFT optimized structures of the theoretical models used for the Au(I)-protein adducts Et_3P-Au(I)-Cys (**I-A**), Cys-Au(I)-Cys (**I-B**), His-Au(I)-His (**I-C**) and Cys-Au(I)-His (**I-D**). Cys was modelled as N-acetyl-N-methylamide-cysteine and His residues were modelled as 5-methylimidazole.

Figure 4 shows a zoom-in of the white line region of the Au L_3-edge XANES of the Au(I) model compounds (**1, 2, 5** and **6**) and the selected interaction products (**2+NCp7** and **2+Sp1**(AuF)), and their corresponding TD-DFT-calculated spectra, respectively. An energy shift of -465 eV was applied to the calculated spectra based on the correlation between experimental and calculated energies. The constant shift is necessary due to the sensitivity to relativistic effects of the 2p core-orbital energies as well as the approximate exchange-correlation potential, which are not perfectly described in our calculations. A broadening of 4.4 eV FWHM, based on the Au $2p_{3/2}$ core-hole lifetime, was used in all calculated spectra. We note that the TD-DFT-calculated spectra can only be expected to capture the edge-region well, but not the post-edge region of the XAS spectra. Overall, the calculated spectra nicely reproduce the observed experimental trends, both in terms of the energies and the intensity distribution. Furthermore, TD-DFT can reveal the nature of the transitions involved. As these are all Au(I) model compounds with formally a full d-electron shell, from an electronic structure point of view *Au 2p* $\rightarrow$*Au 6s* orbital excitations should be the first main contribution to the edge. Analysis of the transitions reveals that the Au 6s orbital mixes strongly with the bound-ligand orbitals in these compounds and the excitations are better described as *Au 2p* $\rightarrow$ *Au-L* σ^*. These excitations make up the main peak in the near edge region of the spectrum of all Au(I) compounds, but higher energy charge-transfer excitations into various empty ligand orbitals, in particular the

phosphorus and sulfur d-shells, contribute as well and broaden the peak or result in a second peak, as in the case of compounds **1**, **2** and Cys-Au-Cys (**I-B**). In the sulfur-containing Au-compounds (**1**, **5**, **I-A and I-B**), the *Au 2p* → *Au-L σ** excitations are shifted to slightly higher energy while the higher intensity of the peak compared to compound **2** can be attributed to additional *Au 2p* → *S d* excitations present (with some mixing with Au 5d orbitals due to covalency), that arise due to the more covalent Au-S bond compared to the less covalent Au-Cl bond. Furthermore, the calculated spectrum of the simple theoretical model (PEt_3)-Au(I)-Cys (**I-A**, Figure 3) is similar to that of compound **6**, in agreement with the experimental spectrum and again supporting our hypothesis that the **2+NCp7** and **6+NCp7** products consist of a P-Au-S local geometry.

In the case of interaction with Sp1, the comparison of the simulated spectra with the experimental ones indicates that either the Cys-Au(I)-Cys (**I-B**) or Cys-Au-His (**I-D**) theoretical motifs are clearly much better models for **2+Sp1** than Et_3P-Au(I)-Cys (**I-A**). The calculated spectra of **I-B** and **I-D** are very similar, with slightly different relative intensities. We also note that the lower energy of the phosphorus d-shell compared to the sulfur d-shell results in a single broad high-intensity peak for the P-Au(I)-S compounds (**6** and **I-A**), while the S-Au-S compounds and S-Au-N compounds (**1, I-B and I-D**) give two peaks (See Fig. 4).

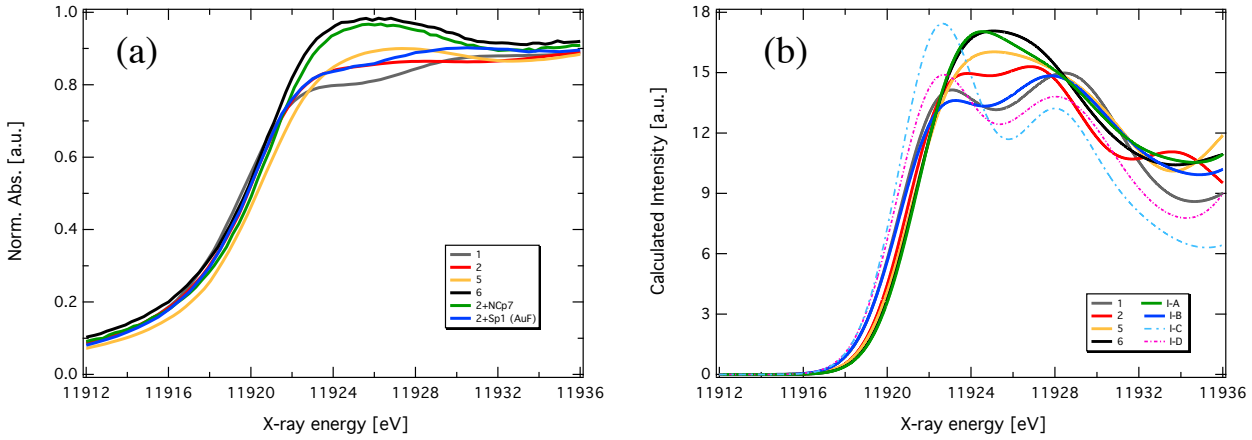

Figure 4. (a) Experimental Au L_3-edge XANES spectra of Au(I) compounds **1**, **2**, **5**, **6**, and interaction products **2+NCp7** and **2+Sp1** (AuF). (b) TD-DFT-calculated L-edge XANES spectra of the same compounds and the proposed models Et_3P-Au-Cys for **2+NCp7** and Cys-Au-Cys and Cys-Au-His for **2+Sp1**. The TD-DFT-calculated spectra have been shifted in energy by -465 eV and broadened by 4.4 eV(FWHM).

Summary. The overall picture in the case of Au(I) compounds interacting with NCp7 and Sp1 zinc fingers is that the gold atom maintains its oxidation state upon interaction, presenting a slightly higher electronic density on the metal center in the case of reaction with Sp1 when compared to NCp7. The stronger donor character of thiols might be responsible for the reduction of the metal center and act in general as a driving force for these reactions. The observation of different products after interaction of **2** with the two zinc fingers is intriguing – why do we observe {AuF} as a dominant species for the Sp1 interaction ? The result may reflect the greater reactivity of the Sp1 core with respect to Zn^{2+} affinity. The binding constants for Zn^{2+} to the two peptides differ significantly with the Zn^{2+} in NCp7 being held much more tightly, which may be general for Cys_3His coordination sites.[29, 76, 77] The {(PEt_3)Au-F} adduct must form (with similar electronic properties to **I-A**), but further reaction on Sp1 may be too fast to observe. The similarities in electronic properties between Cys-Au(I)-Cys (**I-B**) and Cys-Au-His (**I-D**) emphasize that, despite the paradigmatic thiophilicity of Au(I), an important consideration in the intimate mechanisms of substitution of these species may involve initial histidine binding, which has high nucleophilicity and availability in these zinc fingers, especially Sp1F3 (Table S3).[17, 78] In this respect it is notable that ^{31}P NMR studies showed the presence of Au-His binding when auranofin is allowed to react over time with both the C-terminal NCp7 F2 and the fully functional "two-finger" nucleocapsid protein NC.[12] To our knowledge, this is the first Au(I)+ZnF system evaluated by a combination of XAS and TD-DFT. Here, the element-specific technique of XAS combined with the TD-DFT calculations was invaluable in corroborating the hypothesis of electrophilic attack of the metal center (Au(I)) on the cysteine, with replacement of the chloride (compound **2**) and the maintenance of the Et_3P group upon initial reaction with NCp7. This coordination environment has also been observed for the auranofin + bovine serum albumin and auranofin + apo-transferrin systems.[57]

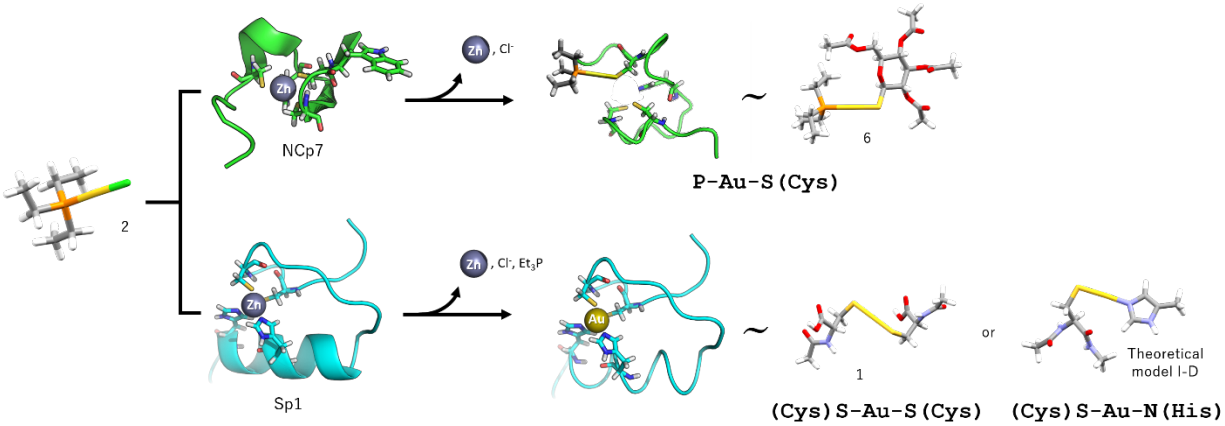

Scheme 1. Reaction of NCp7 and Sp1 with [AuCl(PEt_3)] (compound **2**). The first step is the electrophilic attack of Au(I) to a thiolate. As consequence, the {Et_3PAu} moiety can be identified bound to the apo-peptide as observed for **2+NCp7**. In the final step, the phosphine ligand is lost and another residue from the coordination sphere of Zn (Cys or His) completes the coordination sphere of Au(I), leading to the formation of a *gold finger*. The final coordination sphere of the Au-containing species identified in this study by XAS is highlighted in each case, in comparison to the most similar experimental or theoretical model compound.

Interaction of Au(III) compounds with ZnFs

The XANES spectra of the Au(III) model compounds **10** and **11** are presented in Figures 5(a) and 5(b), respectively, together with the products formed after their interaction with NCp7 and Sp1 zinc fingers. As expected for Au(III) compounds, these spectra contain a strong absorption in the white line region as a consequence of empty Au d orbitals promoting the allowed $2p_{3/2} \rightarrow 5d$ transitions in the L_3-edge XAS. Compounds **10** and **11** have a white line peak located at about 11921 eV with a normalized peak intensity of about 1.2 units.

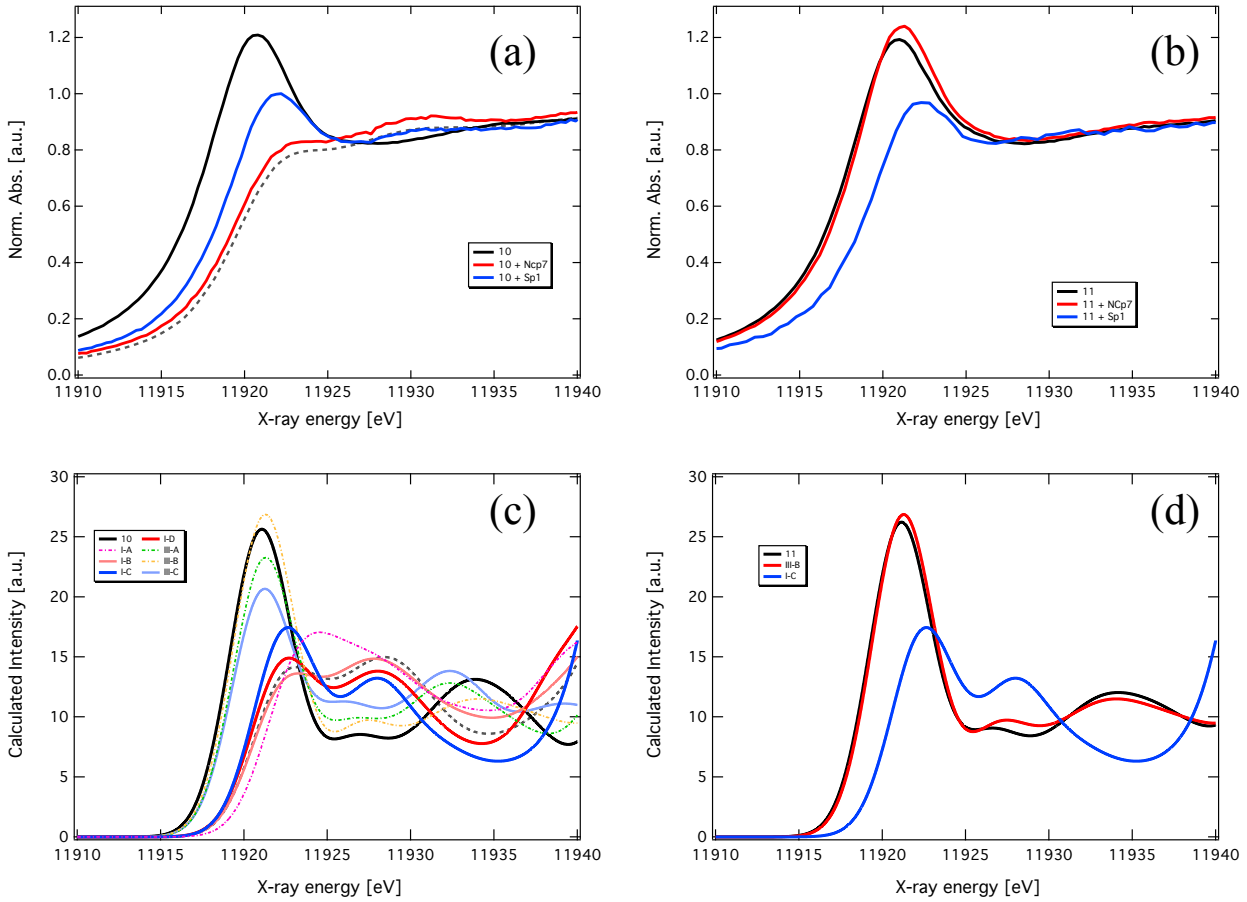

Figure 5. Gold L_3-edge XANES spectra of (a) compound **10** ($[AuCl(dien)]^{2+}$) and its respective reaction products with NCp7 and Sp1 (red and blue, respectively); (b) compound **11** ($[Au(dien)(dmap)]^{3+}$) and its respective reaction products with NCp7 and Sp1 (red and blue, respectively). The spectrum of model compound **1** is also shown (gray dashed line) for comparison. TD-DFT-calculated XANES spectra of (c) the Au(III) compound **10** together with the theoretical models for the Au(III) interaction products with NCp7; (d) the Au(III) compound **11** together with theoretical models (Au(III)(dien)His) (**III-B**) and His-Au(I)-His (**I-C**). The same energy shift of 465 eV was applied to the calculated spectra.

NCp7. The interaction product **10+NCp7** presents an unusual even lower intensity white line, similar to that expected for Au(I) compounds or an even more reduced gold species, thus suggesting that a reduction of Au(III) took place upon the interaction of **10** with NCp7, Figure 5(a). Structurally, **10+NCp7** differs from the model compound $[AuCl(dien)]^{2+}$, as evidenced by both the XANES (Figure 5(a)) and EXAFS (Figure S7) spectra. The XANES of product **10+NCp7** closely resembles that of model compound **1**, presenting a rather weak white line peak, a pronounced post-edge feature at around 11930 eV and another broad one at 11940-11985 eV (Figure 5(a)). For **10+NCp7**, the TD-DFT calculations in fact show that both Cys-Au(I)-Cys

(Figure 3, **I-B**) and Cys-Au(I)-His (Figure 3, **I-D**) theoretical models reproduce the general behaviour observed experimentally, *i.e.*, a diminishing of the white line intensity and an energy shift of about 1.7 eV in the peak position when compared to the spectrum of intact $[AuCl(dien)]^{2+}$ (Figure 5). Both theoretical models indicate that loss of all ligands, Au(III) → Au(I) reduction and coordination to either two cysteine residues or one cysteine and one histidine has occurred upon interaction of $[AuCl(dien)]^{2+}$ with NCp7. If the Au(III) center is reduced, it is likely that two Cys residues will form a disulfide bond (which releases 2 electrons, reducing Au(III) to Au(I)). In the NCp7 case, the two remaining residues are one Cys and one His, which will bind to the Au(I) suggesting Cys-Au(I)-His as the more likely model. In fact, the calculated spectrum of this model gives a slightly higher white line peak intensity than compound **1**, consistent with the experimental observation of **10+NCp7** having slightly higher intensity than compound **1**.

In contrast, the spectrum of reaction product **11+NCp7** (Figure 5(b)) resembles that of its precursor, $[Au(dien)(DMAP)]^{3+}$, with only a slight increase in the white line intensity. Additionally, the EXAFS data of **11+NCp7** and **11** overlaps up to k=8 $Å^{-1}$, which is sufficient to conclude that they have identical first coordination shell around the gold (Figure S9). These results indicate the existence of Au(III) in the initial product with NCp7, contrary to what is observed in the case of **10**. This is in agreement with MS data reported previously, which at early time points shows zinc ejection (apopeptide signal) while signals of $[Au(dien)DMAP]^{3+}$ still persist.[20] Thus, to some extent, Au(III) redox stability was achieved, even in the presence of the rich Cys content of NCp7, by modulating the first coordination sphere of the Au(III)-dien complex. An alternative explanation would be formation of a [Au(dien)(His)] intermediate through the selective electrophilic attack on the histidine residue followed by replacement of DMAP and maintenance of the (dien)Au-N (AuN_4) coordination sphere. The rates of substitution reactions of $[AuCl(dien)]^{2+}$ are very fast in the presence of nac (N-acetyl-cysteine) (< 1 min), but somewhat slower for histidine.[79, 80] Since **11** is more substitution-inert than **10**, it is reasonable to assume the observation of the starting material as the source of the Au(III) species in **11 + NCp7**. The possible mechanisms of reaction of compound **11** are shown in Scheme 2.

Sp1. **10+Sp1** and **11+Sp1** present a well-defined white line peak and the obtained XANES spectra are identical, with the white line peak shifting slightly to higher energies (about

1.4 eV) and reducing its intensity to about 1.0 normalized units, suggesting a change in oxidation state and pointing to the formation of identical species (Figure 5(a), 5(b)). Reaction products **10+Sp1** and **11+Sp1** show experimentally a reduction in white line peak intensity and a slight energy shift and again appear to result in identical products (Figure S9). The spectra differ significantly from the {AuF} reaction product of Sp1 with Au(I).

TD-DFT. TD-DFT-calculated L-edge spectra of different Au(III) models were again fundamental in revealing the nature of the interaction products. Figures 5(c) and 5(d) shows the TD-DFT spectra of compounds **10** and **11** and theoretical models for **10+NCp7, 11+NCp7, 10+Sp1** and **11+Sp1**. The DFT-optimized structures of the theoretical Au(III) models, supplementing the already considered Au(I) models, are presented in Figure 6: **III-A**: (Au(III)(dien)Cys), **III-B**: (Au(III)(dien)His) and **III-C** (Au(III)Cys_2His_2).

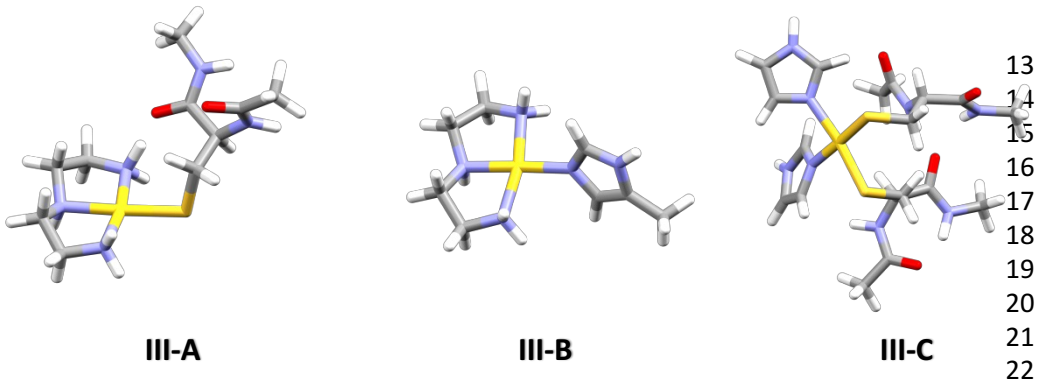

Figure 6. DFT optimized structures of the models used for the reaction products of **10** and **11** with the ZnF proteins. (Au(dien)Cys), **III-A**; (Au(dien)His), **III-B** and (AuCys_2His_2), **III-C**. Cys was modelled as N-acetyl-N-methylamide-cysteine and His residues were modelled as 5-methylimidazole

For comparison with the experimental spectra obained for **10+Sp1** and **11+Sp1**, the theoretical model compounds **I-B, I-C, I-D** , **III-A**, **III-B** and **III-C** were considered. The Au(III) theoretical models do not reproduce the experimental trends observed. For (Au(III)(dien)His), a white line with higher intensity than that observed for compounds **10** and **11** was obtained. The calculated spectrum of model (Au(III)(dien)Cys) shows a rather small reduction in the peak intensity, inconsistent with the *ca*. 20% reduction observed experimentally. The spectrum of the (Au(III)Cys_2His_2) theoretical model reproduces the observed reduction in intensity. However, it does not account for the energy shift observed experimentally, which is

likely a result of Au(III) → Au(I) reduction. The His-Au(I)-His model assumes that the two Cys residues in the Sp1 zinc finger are oxidized to form a disulfide bridge and this electronic transfer reduces Au(III) to Au(I), resulting in ligand loss and binding to the two remaining His residues to Au(I). The calculated XANES spectrum for theoretical model **I-C** accounts for both intensity reduction with respect to the original compounds **10** and **11**, and the correct energy shift in the white line peak. Moreover, the second feature at about 11928 eV is also present in the experimental XAS data of **10+Sp1** and **11+Sp1**, however being slightly broader.

Summary. In the case of Au(III) interactions a rich array of structural motifs is found upon interaction with zinc fingers – dependent both on the nature of the Au(III) species and the zinc finger core. Two principal points to note are that the nature of the {Au(I)F} products formed from reduction of Au(III) are not necessarily the same as those formed directly by the Au(I) compound **2**. Detailed kinetic studies on the reaction of monofunctional gold chelates such as $[AuCl(dien)]^{2+}$ and congeners as well as $[AuCl_4]^-$ with methionine identified a substitution step prior to reduction.[79, 80] The nature of substitution on a peptide template is likely to be very different than for simple amino acids and the differences in final products between the Au(I) and Au(III) species studied here suggest that this may be due to a first substitution reaction on the zinc finger template followed by reduction.

The second point of note is the clear observation for compound **11** of the stabilization of Au(III) at early time points with retention of coordination sphere, the first demonstrated evidence for a "non-covalent" interaction of molecular recognition between **11** and NCp7. Earlier MS studies show that the Zn(II) ion is indeed ejected in the interaction product **11+NCp7**.[17] The structural distinction, besides the differences in substitution kinetics of the Cl^- *versus* N-heterocycle ligand, is the ability of the DMAP ligand to potentially stack with the tryptophan moiety in NCp7, the initial step in the 11+NCp7 recognition.[20] We were also able to identify the non-covalent adduct between compound **11** with the complete "two-finger" nucleocapsid NC (Zn_2F) by MS, further supporting the importance of an initially π-stacked species in the recognition of $[Au(dien)(DMAP)]^{3+}$ by NCp7, Figure S10. We recently demonstrated that both **11** and its purine analog $[Au(dien)(9\text{-ethylguanine})]^{3+}$, inhibit the interaction of the "full" zinc finger with a small model for its natural substrate, SL2 RNA, and display moderate ability to inhibit HIV infectivity.[27] The unique behavior of **11** from the XAS data suggests that inhibition

of the "full" NC(Zn_2F) – SL2 DNA interaction may involve initially a "non-covalent" zinc ejection mechanism driven by the DMAP-tryptophan recognition.[4] Coordination compounds, such as those described here, could be used to examine the role of π-π stacking in stabilization or maintenance of the zinc coordination sphere in nucleocapsid protein-oligonucleotide interactions.[4, 5]

Zinc K-edge XAS

The zinc K-edge XAS of the ZnFs before and after the interaction with gold compounds (Zn ejectors) can be a powerful tool to get insight about mechanism of interaction by probing the ejected zinc species. Indeed, zinc EXAFS has been previously used to structurally characterize ZnF binding sites in NCp7 and in the N-terminal domain of HIV-2-integrase.[81, 82] Two element edges XAS (Au L_3-edge and Zn K-edge) were used in the present case to examine the substitution reactions of Zn ions from the peptide cores. The Zn K-edge XANES of the free ZnF proteins NCp7 and Sp1 are shown in Figure 7, together with those from the reaction products obtained from the interaction with the Au(I) and Au(III) model compounds, **2**, **10** and **11**, respectively. Initially, the XANES spectra of the free NCp7 and Sp1 proteins are identical, with a small intensity mismatch in the white line region that can be due to minor different scattering properties between the two proteins. This confirms that, despite the differences in the protein core (Sp1: Cys_2His_2 and NCp7: Cys_3His), the electronic density and chemical/geometrical environment around the Zn(II) atoms are similar.

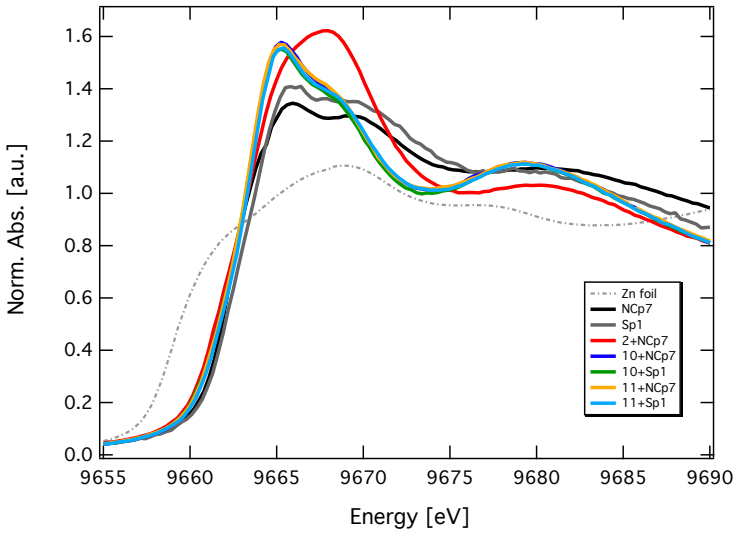

Figure 7. Zinc K-edge XANES spectra of the pure NCp7 (black) and Sp1 (gray) proteins, and the interaction products with Au(I) compound **2+NCp7** (red) and Au(III) compounds **10+NCp7** (blue), **10+Sp1** (green), **11+NCp7** (orange) and **11+Sp1** (cyan).

The changes in the Zn K-edge XANES upon interaction of **2** with NCp7 indicate a complete modification of the zinc environment, Figure 7. Likewise, after the interaction of NCp7 and Sp1 with Au(III) model compounds **10** and **11**, the spectra change significantly, in particular in the near-edge region around 9665-9700 eV. Again, this evidences a significant rearrangement of the zinc coordination shell after interaction of the Au(III) compounds with the ZnF proteins. The Zn K-edge spectra of the reaction products after the interaction of Au(III) compounds with the proteins are also identical among themselves and different from that obtained after the interaction with Au(I). Hence, the specific zinc species formed is dependent on whether Au(I) or Au(III) is used in the perturbation of the structure. This observation can reflect that some gold compounds can promote the formation of intermediate species with Zn(II) partially coordinated to the protein, or the ligands (mainly the nitrogen donors) can help the promotion of zinc ejection by coordinating zinc. However, additional analyses and modelling are necessary to understand the complexation of the released zinc. Given the structural adaptability of zinc binding sites in proteins, a structural model for the eventually displaced Zn species will be subject of future studies.

Conclusions

The use of model compounds combined with data from the natural protein systems is an extremely powerful approach to the analysis of metal ion oxidation state and structure in metalloproteins. The identification of the oxidation state of Mo in the FeMoco cluster of nitrogenase is perhaps a paradigmatic example.[68, 83] The study of model Au(I) and Au(III) compounds, combined with TD-DFT on theoretical products and with dual-element Au,Zn XAS has allowed a description of the early stages of these reactions with zinc finger peptides. What is clear is that with multiple possible binding sites on the zinc coordination sphere, the pathways for production of even a superficially simple species such as {AuF} are rich and diverse. The coordination sphere of the final Au-containing protein depends on the initial oxidation state of

Au in metal complex evaluated (Au(I) vs Au(III)) and also on the intrinsic reactivity of protein (NCp7 vs Sp1). For the Au(III) compounds studied here (**10** and **11**), the fact that the final interaction products with NCp7 and Sp1 are not the same as observed for the Au(I) compounds, is indicative of an important ligand-replacement step prior to reduction. In general, for Au(III) complexes with the right ligands (chelators, strong σ-donors), the redox process can be slowed down and ligand replacement will start to be relevant.

In the Au(III) cases where reduction takes place (**10**+NCp7, **10**+Sp1 and **11**+Sp1), a mechanism can also be generalized. We can assume the oxidation of two of the available Cys residues in the protein, with formation of a disulfide bond, and coordination of the two remaining residues to Au(I). With this in mind, the final coordination sphere is suggested to be (Cys)S-Au-N(His) for **10**+NCp7 and (His)N-Au-N(His) for **10**+Sp1 and **11**+Sp1. Selectivity towards His coordination in the Au(III) case can also be supported based on the higher stability of the initial Au(III)-N(His) bond, taking into account the harder Lewis acid character of Au(III) vs Au(I). Examination of the electrostatic potential of the Zn-binding ligands allied to their *accessibility* also suggests that we may be observing kinetic *versus* thermodynamic preferences when we consider the final products, Table S3. While much emphasis in targeting zinc fingers has emphasised thiophilic agents[22,23], the results presented here suggest that histidine is a competitive residue susceptible to modification by Lewis acid electrophiles. Finally, the interaction between 11+NCp7 was particularly unique, in that Zn displacement was observed based on the Zn K-edge XAS while the L3-edge Au XAS was of the interaction product (11+NCp7) was almost identical with the free compound (11). These results clearly suggest retention of the Au(III) oxidation state and the AuN_4 coordination sphere, which could correspond to either [Au(dien)(DMAP)] or [Au(dien)(His)] species (Scheme 2). The kinetics of substitution by His are likely to be slow[79,80] but nevertheless the possibility cannot be discarded at this point. In support of the retention of the coordination sphere, mass spectrometric data (Figure S10) does show a possible non-covalent intermediate formed by the interaction of 11 and the fully functional HIV nucleocapsid protein.

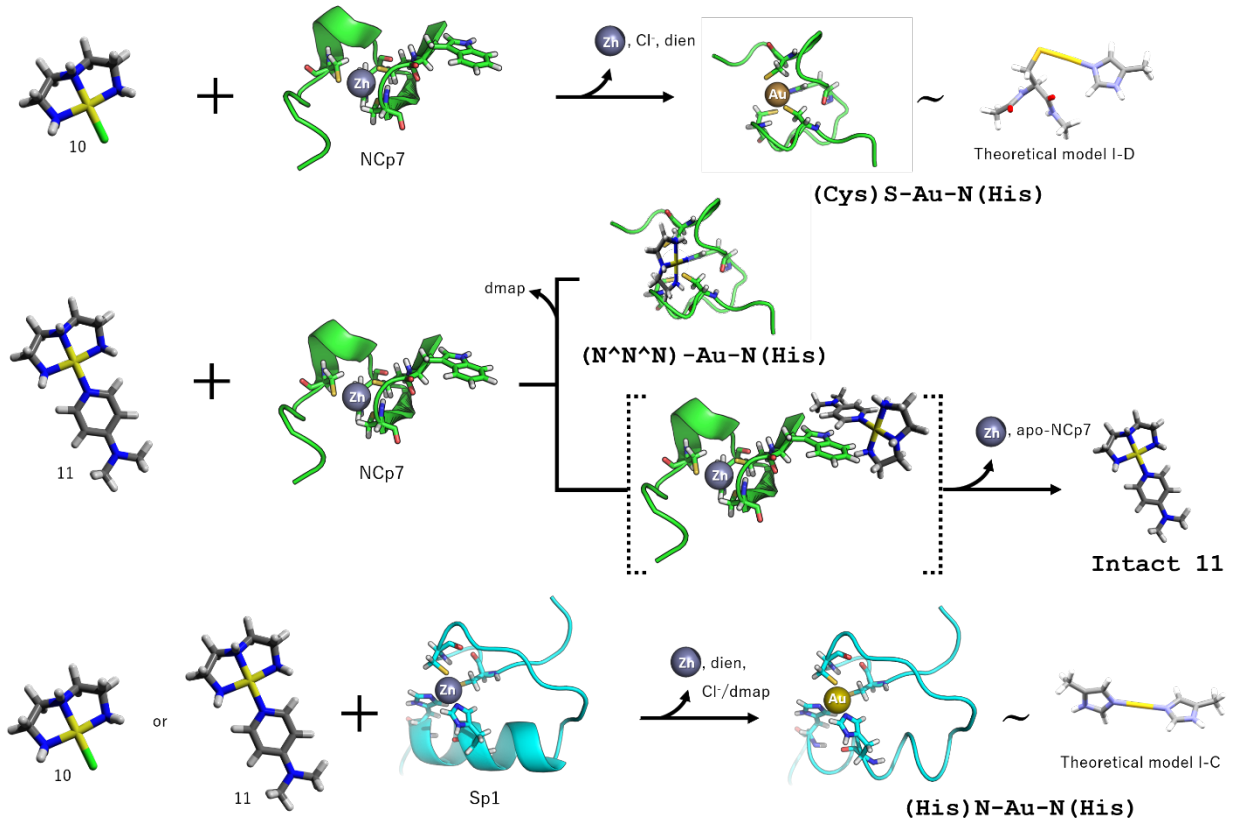

Scheme 2. Reaction of zinc fingers NCp7 and Sp1 with $[AuCl(dien)]^{2+}$ (compound **10**) and $[Au(dien)(DMAP)]^{3+}$ (compound **11**). Zinc ion is replaced by Au complexes with and without ligand loss. The final coordination sphere of Au is highlighted in each case. Reduction and incorporation of Au(I) to the protein is the typical behavior. On the other hand, for the reaction **11**+NCp7, Au(III) is present in product.

In summary, we demonstrated that a combination of XAS and TD-DFT calculations can be a powerful tool to complement other spectroscopic techniques allowing the elucidation of the coordination sphere and oxidation state of Au(I,III) compounds upon reaction with zinc fingers. The ability to probe both gold and zinc metal centers independently is particularly desirable in these cases as the coordination sphere and oxidation state of the metal might not be directly and simultaneously assessed by routine techniques such as UV-Vis, NMR and MS spectroscopies. The XAS results bring additional structural information on these systems besides spectroscopic and mass spectral techniques and help suggest limiting mechanisms for structurally distinct zinc fingers. The intimate mechanism of Au-Cys formation could in principle arise from nucleophilic attack of a zinc-bound thiolate with concomitant loss of Zn or direct attack of a thiolate ligand after dissociation from the Zn coordination sphere. Dinuclear cysteine-bridged species, possible

in a multi-cysteine system such as a zinc finger, have been observed in reactions of Au(I)(PR_3) compounds with N-AcCys.[17] Further studies including time course of the reactions followed by XAS could help elucidate some of these points.

Conflicts of Interest. The authors declare no conflicts of interest.

Supporting Information Available

Experimental and TD-DFT calculated XANES of the Au(I) and Au(III) model compounds, Table of edge positions, EXAFS of the interaction of Au(I) compounds with ZF, MS spectrum of the interaction of Au(I) compounds with ZF, EXAFS of the interaction of Au(III) compounds with ZF, experimental XANES of the interaction of Au(III) compounds with ZF, MS of the interaction of Au(III) compounds with ZF, STING descriptors of ZF.

Acknowledgements

This work was supported by National Science Foundation NSF CHE-1413189; São Paulo Research Foundation (FAPESP) 2014/20334-0 and 2015/9905-1, Brazilian Federal Agency for the Support and Evaluation of Graduate Education (CAPES), CAPES/PVES 154/2012 and 0580/2013. We thank the Brazilian Synchrotron Light Laboratory for the beamtime and the XAFS1 and XAFS2 staff for the support. We specially thank Anna Paula Sotero and Carlos Doro Neto for the technical support at the synchrotron beamlines. FAL acknowledges National Council for Scientific and Technological Development (CNPq) for the productivity grant number 311270/2015-8". CA acknowledges support from FAPESP 2013/20334-0 and Brazilian Synchrotron Light Laboratory LNLS 1- XAFS1-17707 and LNLS2 research project 2015 0089. RB acknowledges support from the Icelandic Research Fund, Grant No. 141218051 and the University of Iceland Research Fund.

References

1. Jen, J.; Wang, Y.-C. Zinc finger proteins in cancer progression. *J Biomed Sci* **2016,** *23*, 53-62.

2. Yang, C.; Huang, S.; Wang, X.; Gu, Y. Emerging Roles of CCCH-Type Zinc Finger Proteins in Destabilizing mRNA Encoding Inflammatory Factors and Regulating Immune Responses. *Crit Rev Eukaryot Gene Expr* **2015,** *25*, 77-89.

3. Fu, M.; Blackshear, P. J. RNA-binding proteins in immune regulation: a focus on CCCH zinc finger proteins. *Nat Rev Immunol* **2017,** *17*, 130-143.

4. Garg, D.; Torbett, B. E. Advances in targeting nucleocapsid-nucleic acid interactions in HIV-1 therapy. *Virus Res* **2014,** *193*, 135-143.

5. Mori, M.; Kovalenko, L.; Lyonnais, S.; Antaki, D.; Torbett, B. E.; Botta, M.; Mirambeau, G.; Mely, Y. Nucleocapsid Protein: A Desirable Target for Future Therapies Against HIV-1. *Curr Top Microbiol Immunol* **2015,** *389*, 53-92.

6. Klug, A. The discovery of zinc fingers and their applications in gene regulation and genome manipulation. *Annu Rev Biochem* **2010,** *79*, 213-231.

7. Quintal, S. M.; dePaula, Q. A.; Farrell, N. P. Zinc finger proteins as templates for metal ion exchange and ligand reactivity. Chemical and biological consequences. *Metallomics* **2011,** *3*, 121-139.

8. Matosziuk, L. M.; Holbrook, R. J.; Manus, L. M.; Heffern, M. C.; Ratner, M. A.; Meade, T. J. Rational design of [Co(acacen)L2]+ inhibitors of protein function. *Dalton Trans* **2013,** *42*, 4002-4012.

9. Tsotsoros, S. D.; Lutz, P. B.; Daniel, A. G.; Peterson, E. J.; de Paiva, R. E. F.; Rivera, E.; Qu, Y.; Bayse, C. A.; Farrell, N. P. Enhancement of the physicochemical properties of [Pt(dien)(nucleobase)]2+ for HIVNCp7 targeting. *Chem Sci* **2017,** *8*, 1269-1281.

10. Ndagi, U.; Mhlongo, N.; Soliman, M. E. Metal complexes in cancer therapy - an update from drug design perspective. *Drug Des Devel Ther* **2017,** *11*, 599-616.

11. Jürgens, S.; Casini, A. Mechanistic Insights into Gold Organometallic Compounds and their Biomedical Applications. *CHIMIA International Journal for Chemistry* **2017,** *71*, 92-101.

12. Djekovic, A.; Petrovic, B.; Bugarcic, Z. D.; Puchta, R.; van Eldik, R. Kinetics and mechanism of the reactions of Au(iii) complexes with some biologically relevant molecules. *Dalton Trans* **2012,** *41*, 3633-3641.

13. Larabee, J. L.; Hocker, J. R.; Hanas, J. S. Mechanisms of Aurothiomalate and Cys2His2 Zinc Finger Interactions. *Chem Res Toxicol* **2005,** *18*, 1943-1954.

14. Franzman, M. A.; Barrios, A. M. Spectroscopic Evidence for the Formation of Goldfingers. *Inorg Chem* **2008,** *47*, 3928-3930.

15. Handel, M. L.; deFazio, A.; Watts, C. K.; Day, R. O.; Sutherland, R. L. Inhibition of DNA binding and transcriptional activity of a nuclear receptor transcription factor by aurothiomalate and other metal ions. *Mol Pharmacol* **1991,** *40*, 613-618.

16. Abbehausen, C.; Peterson, E. J.; de Paiva, R. E. F.; Corbi, P. P.; Formiga, A. L. B.; Yun, Q.; Farrell, N. P. Gold(I)-Phosphine-N-Heterocycles: Biological Activity and Specific (Ligand) Interactions on the C-Terminal HIVNCp7 Zinc Finger. *Inorg Chem* **2013,** *52*, 11280-11287.

17. de Paiva, R. E. F.; Du, Z.; Peterson, E.J.; Corbi, P.P.; Farrell, N. P. Probing the HIV-1 NCp7 nucleocapsid protein with site-specific gold(I)-phosphine complexes. *Inorg. Chem.* **2017**, *129*, 4535-4538.

18. de Paula, Q. A.; Mangrum, J. B.; Farrell, N. P. Zinc finger proteins as templates for metal ion exchange: Substitution effects on the C-finger of HIV nucleocapsid NCp7 using M(chelate) species (M=Pt, Pd, Au). *J Inorg Biochem* **2009,** *103*, 1347-1354.

19. Spell, S. R.; Farrell, N. P. Synthesis and Properties of the First $[Au(dien)(N\text{-heterocycle})]^{3+}$ Compounds. *Inorg Chem* **2014,** *53*, 30-32.

20. Spell, S. R.; Farrell, N. P. $[Au(dien)(N\text{-heterocycle})]^{3+}$: Reactivity with Biomolecules and Zinc Finger Peptides. *Inorg Chem* **2015,** *54*, 79-86.

21. Jacques, A.; Lebrun, C.; Casini, A.; Kieffer, I.; Proux, O.; Latour, J. M.; Seneque, O. Reactivity of Cys4 Zinc Finger Domains with Gold(III) Complexes: Insights into the Formation of "Gold Fingers". *Inorg Chem* **2015,** *54*, 4104-4113.

22. Meier, S. M.; Gerner, C.; Keppler, B. K.; Cinellu, M. A.; Casini, A. Mass Spectrometry Uncovers Molecular Reactivities of Coordination and Organometallic Gold(III) Drug Candidates in Competitive Experiments That Correlate with Their Biological Effects. *Inorg Chem* **2016,** *55*, 4258-4259.

23. Laskay, U. A.; Garino, C.; Tsybin, Y. O.; Salassa, L.; Casini, A. Gold finger formation studied by high-resolution mass spectrometry and in silico methods. *Chem Commun* **2015,** *51*, 1612-1615.

24. Serratrice, M.; Edafe, F.; Mendes, F.; Scopelliti, R.; Zakeeruddin, S. M.; Graetzel, M.; Santos, I.; Cinellu, M. A.; Casini, A. Cytotoxic gold compounds: synthesis, biological characterization and investigation of their inhibition properties of the zinc finger protein PARP-1. *Dalton Trans* **2012,** *41*, 3287-3293.

25. Maynard, A. T.; Covell, D. G. Reactivity of Zinc Finger Cores: Analysis of Protein Packing and Electrostatic Screening. *J Am Chem Soc* **2001,** *123*, 1047-1058.

26. Maynard, A. T.; Huang, M.; Rice, W. G.; Covell, D. G. Reactivity of the HIV-1 nucleocapsid protein p7 zinc finger domains from the perspective of density-functional theory. *Proc Natl Acad Sci USA* **1998,** *95*, 11578-11583.

27. Spell, S. R.; Mangrum, J. B.; Peterson, E. J.; Fabris, D.; Ptak, R.; Farrell, N. P. Au(III) compounds as HIV nucleocapsid protein (NCp7)-nucleic acid antagonists. *Chem Commun* **2017,** *53*, 91-94.

28. Tiekink, E. Chloro(triethylphosphine)gold(I). *Acta Cryst Sect C Cryst Struct Commun* **1989,** *45*, 1233-1234.

29. Grant, T. A.; Forward, J. M.; Fackler, J. P. Crystal structure of 2-mercapto-2-thiazoline(triphenylphosphine)gold(I), [Au(C3H4NS2)P(C6H5)3]. *Z Kristallogr* **1996,** *211*, 483-484.

30. Corbi, P. P.; Quintao, F. A.; Ferraresi, D. K. D.; Lustri, W. R.; Amaral, A. C.; Massabni, A. C. Chemical, spectroscopic characterization, and in vitro antibacterial studies of a new gold(I) complex with N-acetyl-L-cysteine. *J Coord Chem* **2010,** *63*, 1390-1397.

31. Rosenzweig, A.; Cromer, D. T. The crystal structure of $KAu(CN)_2$. *Acta Cryst* **1959,** *12*, 709-712.

32. Bonamico, M.; Dessy, G. The crystal structure of anhydrous potassium tetrachloroaurate(III). *Acta Cryst B Struct Sci* **1973,** *29*, 1735-1736.

33. Baenziger, N. C.; Bennett, W. E.; Soborofe, D. M. Chloro(triphenylphosphine)gold(I). *Acta Cryst B* **1976,** *32*, 962-963.

34. Horvath, U. E. I.; Cronje, S.; Nogai, S. D.; Raubenheimer, H. G. A second polymorph of (2-thiazolidinethionato)(triphenylphosphine)gold(I). *Acta Cryst E Struct Rep Online* **2006,** *62*, m1641-m1643.

35. Horvath, U. E. I.; Raubenheimer, H. G. A third polymorph of (2-thiazolidinethionato)(triphenylphosphine)gold(I). *Acta Cryst E Struct Rep Online* **2006,** *62*, m1644-m1645.

36. Jones, P. G.; Lautner, J. Redetermination of the structure of cyano(triphenylphosphine)gold(I). *Acta Cryst Sect C Cryst Struct Commun* **1988,** *C44*, 2091-2093.

37. Hill, D. T.; Sutton, B. M. (2,3,4,6-Tetra-O-acetyl-1-thio-β-D-glucopyranosato-S) (triethylphosphine)gold, C20H34AuO9PS. *Cryst Struct Commun* **1980,** *9*, 679-686.

38. Figueroa, S. J. A.; Mauricio, J. C.; Murari, J.; Beniz, D. B.; Piton, J. R.; Slepicka, H. H.; Sousa, M. F. d.; Espíndola, A. M.; Levinsky, A. P. S. Upgrades to the XAFS2 beamline control system and to the endstation at the LNLS. *Journal of Physics: Conference Series* **2016,** *712*, 012022.

39. Ravel, B.; Newville, M. Athena, Artemis, Hephaestus: data analysis for X-ray absorption spectroscopy using IFEFFIT. *J Synchrotron Rad* **2005,** *12*, 537-541.

40. Tolentino, H. C. N.; Ramos, A. Y.; Alves, M. C. M.; Barrea, R. A.; Tamura, E.; Cezar, J. C.; Watanabe, N. A 2.3 to 25 keV XAS beamline at LNLS. *J Synchrotron Rad* **2001,** *8*, 1040-1046.

41. Neese, F. The ORCA program system. *Wiley Interdiscip Rev Comput Mol Sci* **2012,** *2*, 73-78.

42. Weigend, F.; Ahlrichs, R. Balanced basis sets of split valence, triple zeta valence and quadruple zeta valence quality for H to Rn: Design and assessment of accuracy. *PCCP* **2005,** *7*, 3297-3305.

43. Petrenko, T.; Kossmann, S.; Neese, F. Efficient time-dependent density functional theory approximations for hybrid density functionals: Analytical gradients and parallelization. *J Chem Phys* **2011,** *134*, 054116.

44. Perdew, J. P.; Ernzerhof, M.; Burke, K. Rationale for mixing exact exchange with density functional approximations. *J Chem Phys* **1996,** *105*, 9982-9985.

45. Perdew, J. P.; Burke, K.; Ernzerhof, M. Generalized Gradient Approximation Made Simple. *Phys Rev Lett* **1996,** *77*, 3865-3868.

46. Jansen, G.; Hess, B. A. Revision of the Douglas-Kroll transformation. *Phys Rev A* **1989,** *39*, 6016-6017.

47. Hess, B. A. Relativistic electronic-structure calculations employing a two-component no-pair formalism with external-field projection operators. *Phys Rev A* **1986,** *33*, 3742-3748.

48. Samzow, R.; Hess, B. A.; Jansen, G. The two-electron terms of the no-pair Hamiltonian. *J Chem Phys* **1992,** *96*, 1227-1231.

49. Pantazis, D. A.; Chen, X.-Y.; Landis, C. R.; Neese, F. All-Electron Scalar Relativistic Basis Sets for Third-Row Transition Metal Atoms. *J Chem Theory Comput* **2008,** *4*, 908-919.

50. Izsák, R.; Neese, F. An overlap fitted chain of spheres exchange method. *J Chem Phys* **2011,** *135*, 144105.

51. Neese, F.; Wennmohs, F.; Hansen, A.; Becker, U. Efficient, approximate and parallel Hartree–Fock and hybrid DFT calculations. A 'chain-of-spheres' algorithm for the Hartree–Fock exchange. *Chem Phys* **2009,** *356*, 98-109.

52. Neshich, G.; Togawa, R. C.; Mancini, A. L.; Kuser, P. R.; Yamagishi, M. E. B.; Pappas, G.; Torres, W. V.; Campos, T. F. e.; Ferreira, L. L.; Luna, F. M.; Oliveira, A. G.; Miura, R. T.; Inoue, M. K.; Horita, L. G.; de Souza, D. F.; Dominiquini, F.; Álvaro, A.; Lima, C. S.; Ogawa, F. O.; Gomes, G. B.; Palandrani, J. F.; dos Santos, G. F.; de Freitas, E. M.; Mattiuz, A. R.; Costa, I. C.; de Almeida, C. L.; Souza, S.; Baudet, C.; Higa, R. H. STING Millennium: a web-based suite of programs for comprehensive and simultaneous analysis of protein structure and sequence. *Nucleic Acids Res* **2003,** *31*, 3386-3392.

53. Sridharan, S.; Nicholls, A.; Honig, B. A new vertex algorithm to calculate solvent accessible surface areas. *Biophys J* **1992,** *61*, A174.

54. Honig, B.; Nicholls, A. Classical electrostatics in biology and chemistry. *Science* **1995,** *268*, 1144-1149.

55. Rocchia, W.; Sridharan, S.; Nicholls, A.; Alexov, E.; Chiabrera, A.; Honig, B. Rapid grid-based construction of the molecular surface and the use of induced surface charge to calculate reaction field energies: Applications to the molecular systems and geometric objects. *J Comput Chem* **2002,** *23*, 128-137.

56. Neshich, G.; Rocchia, W.; Mancini, A. L.; Yamagishi, M. E. B.; Kuser, P. R.; Fileto, R.; Baudet, C.; Pinto, I. P.; Montagner, A. J.; Palandrani, J. F.; Krauchenco, J. N.; Torres, R. C.; Souza, S.; Togawa, R. C.; Higa, R. H. JavaProtein Dossier: a novel web-based data visualization tool for comprehensive analysis of protein structure. *Nucleic Acids Res* **2004,** *32*, W595-W601.

57. Messori, L.; Balerna, A.; Ascone, I.; Castellano, C.; Gabbiani, C.; Casini, A.; Marchioni, C.; Jaouen, G.; Congiu Castellano, A. X-ray absorption spectroscopy studies of the adducts formed between cytotoxic gold compounds and two major serum proteins. *J Biol Inorg Chem* **2011,** *16*, 491-499.

58. Lu, Z. H.; Sham, T. K.; Vos, M.; Bzowski, A.; Mitchell, I. V.; Norton, P. R. Unoccupieddstates of Au impurities in silicon as studied by x-ray-absorption spectroscopy. *Phys Rev B* **1992,** *45*, 8811-8814.

59. Chang, S. Y.; Molleta, L. B.; Booth, S. G.; Uehara, A.; Mosselmans, J. F. W.; Ignatyev, K.; Dryfe, R. A. W.; Schroeder, S. L. M. Automated analysis of XANES: A feasibility study of Au reference compounds. *Journal of Physics: Conference Series* **2016,** *712*, 012070.

60. Chang, S.-Y.; Uehara, A.; Booth, S. G.; Ignatyev, K.; Mosselmans, J. F. W.; Dryfe, R. A. W.; Schroeder, S. L. M. Structure and bonding in Au(i) chloride species: a critical examination of X-ray absorption spectroscopy (XAS) data. *RSC Adv* **2015,** *5*, 6912-6918.

61. Abbehausen, C.; Manzano, C. M.; Corbi, P. P.; Farrell, N. P. Effects of coordination mode of 2-mercaptothiazoline on reactivity of Au(I) compounds with thiols and sulfur-containing proteins. *J Inorg Biochem* **2016,** *165*, 136-145.

62. Shaw, C. F. Gold-based therapeutic agents. *Chem Rev* **1999,** *99*, 2589-2600.

63. Elder, R. C.; Zhao, Z.; Zhang, Y.; Dorsey, J. G.; Hess, E. V.; Tepperman, K. Dicyanogold (I) is a common human metabolite of different gold drugs. *J Rheumatol* **1993,** *20*, 268-272.

64. Rehr, J. J.; Albers, R. C. Theoretical approaches to x-ray absorption fine structure. *Rev Mod Phys* **2000,** *72*, 621-654.

65. Westre, T. E.; Kennepohl, P.; DeWitt, J. G.; Hedman, B.; Hodgson, K. O.; Solomon, E. I. A Multiplet Analysis of Fe K-Edge 1s → 3d Pre-Edge Features of Iron Complexes. *J Am Chem Soc* **1997,** *119*, 6297-6314.

66. van der Veen, R. M.; Kas, J. J.; Milne, C. J.; Pham, V.-T.; Nahhas, A. E.; Lima, F. A.; Vithanage, D. A.; Rehr, J. J.; Abela, R.; Chergui, M. L-edge XANES analysis of photoexcited metal complexes in solution. *PCCP* **2010,** *12*, 5551-5561.

67. Alperovich, I.; Smolentsev, G.; Moonshiram, D.; Jurss, J. W.; Concepcion, J. J.; Meyer, T. J.; Soldatov, A.; Pushkar, Y. Understanding the Electronic Structure of 4d Metal Complexes: From Molecular Spinors to L-Edge Spectra of a di-Ru Catalyst. *J Am Chem Soc* **2011,** *133*, 15786-15794.

68. Bjornsson, R.; Lima, F. A.; Spatzal, T.; Weyhermller, T.; Glatzel, P.; Bill, E.; Einsle, O.; Neese, F.; Debeer, S. Identification of a spin-coupled Mo(iii) in the nitrogenase ironmolybdenum cofactor. *Chem Sci* **2014,** *5*, 3096-3103.

69. DeBeer George, S.; Petrenko, T.; Neese, F. Prediction of Iron K-Edge Absorption Spectra Using Time-Dependent Density Functional Theory. *J Phys Chem A* **2008,** *112*, 12936-12943.

70. Hugenbruch, S.; Shafaat, H. S.; Kramer, T.; Delgado-Jaime, M. U.; Weber, K.; Neese, F.; Lubitz, W.; DeBeer, S. In search of metal hydrides: an X-ray absorption and emission study of [NiFe] hydrogenase model complexes. *PCCP* **2016,** *18*, 10688-10699.

71. Kowalska, J. K.; Hahn, A. W.; Albers, A.; Schiewer, C. E.; Bjornsson, R.; Lima, F. A.; Meyer, F.; DeBeer, S. X-ray Absorption and Emission Spectroscopic Studies of [L2Fe2S2]n Model Complexes: Implications for the Experimental Evaluation of Redox States in Iron–Sulfur Clusters. *Inorg Chem* **2016,** *55*, 4485-4497.

72. Lima, F. A.; Bjornsson, R.; Weyhermller, T.; Chandrasekaran, P.; Glatzel, P.; Neese, F.; Debeer, S. High-resolution molybdenum K-edge X-ray absorption spectroscopy analyzed with time-dependent density functional theory. *PCCP* **2013,** *15*, 20911-20920.

73. Rees, J. A.; Wandzilak, A.; Maganas, D.; Wurster, N. I. C.; Hugenbruch, S.; Kowalska, J. K.; Pollock, C. J.; Lima, F. A.; Finkelstein, K. D.; DeBeer, S. Experimental and theoretical correlations

between vanadium K-edge X-ray absorption and K-beta emission spectra. *J Biol Inorg Chem* **2016,** *21*, 793-805.

74. Roemelt, M.; Beckwith, M. A.; Duboc, C.; Collomb, M.-N.; Neese, F.; DeBeer, S. Manganese K-Edge X-Ray Absorption Spectroscopy as a Probe of the Metal–Ligand Interactions in Coordination Compounds. *Inorg Chem* **2012,** *51*, 680-687.

75. Bjornsson, R.; Delgado-Jaime, M. U.; Lima, F. A.; Sippel, D.; Schlesier, J.; Weyhermüller, T.; Einsle, O.; Neese, F.; DeBeer, S. Molybdenum L-Edge XAS Spectra of MoFe Nitrogenase. *Z Anorg Allg Chem* **2015,** *641*, 65-71.

76. Mély, Y.; De Rocquigny, H.; Morellet, N.; Roques, B. P.; Gérard, D. Zinc Binding to the HIV-1 Nucleocapsid Protein: A Thermodynamic Investigation by Fluorescence Spectroscopy. *Biochemistry* **1996,** *35*, 5175-5182.

77. Posewitz, M. C.; Wilcox, D. E. Properties of the Sp1 Zinc Finger 3 Peptide: Coordination Chemistry, Redox Reactions, and Metal Binding Competition with Metallothionein. *Chem Res Toxicol* **1995,** *8*, 1020-1028.

78. Du, Z.; De Paiva, R. E. F.; Qu, Y.; Farrell, N. Tuning the reactivity of Sp1 zinc fingers with platinum complexes. *Dalton Trans* **2016,** *45*, 8712-8716.

79. Durovic, M. D.; Bugarcic, Z. D.; Heinemann, F. W.; van Eldik, R. Substitution versus redox reactions of gold(iii) complexes with l-cysteine, l-methionine and glutathione. *Dalton Trans* **2014,** *43*, 3911-3921.

80. Glisic, B. D.; Rychlewska, U.; Djuran, M. I. Reactions and structural characterization of gold(III) complexes with amino acids, peptides and proteins. *Dalton Trans* **2012,** *41*, 6887-6901.

81. Summers, M. F.; Henderson, L. E.; Chance, M. R.; South, T. L.; Blake, P. R.; Perez-Alvarado, G.; Bess, J. W.; Sowder, R. C.; Arthur, L. O.; Sagi, I. Nucleocapsid zinc fingers detected in retroviruses: EXAFS studies of intact viruses and the solution-state structure of the nucleocapsid protein from HIV-1. *Protein Sci* **1992,** *1*, 563-574.

82. Feiters, M. C.; Eijkelenboom, A. P. A. M.; Nolting, H.-F.; Krebs, B.; van den Ent, F. M. I.; Plasterk, R. H. A.; Kaptein, R.; Boelens, R. X-ray absorption spectroscopic studies of zinc in the N-terminal domain of HIV-2 integrase and model compounds. *J Synchrotron Rad* **2003,** *10*, 86-95.

83. Kowalska, J.; DeBeer, S. The role of X-ray spectroscopy in understanding the geometric and electronic structure of nitrogenase. *Biochim Biophys Acta* **2015,** *1853*, 1406-1415.

FOR TABLE OF CONTENTS ONLY

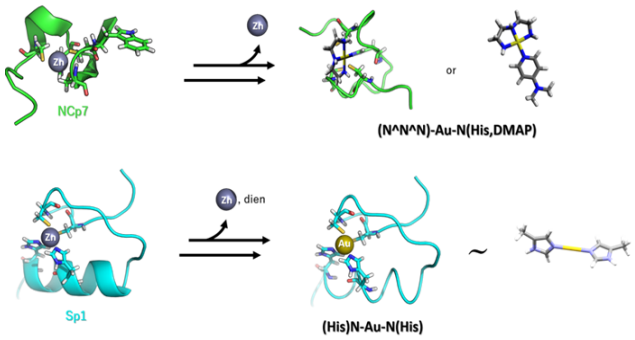

X-Ray Absorption Spectroscopy combined with DFT delineates differential stepwise reactions and binding modes of Au(I) and Au(III) on zinc finger templates